On the potential of linked-basin tidal power plants: an operational and coastal modelling assessment

Athanasios Angeloudis[a,b,*], Stephan C. Kramer[b], Noah Hawkins[b], Matthew D. Piggott[b]

[a] *School of Engineering, Institute for Infrastructure and the Environment, University of Edinburgh, UK*
[b] *Department of Earth Science & Engineering, Imperial College London, UK*

Abstract

Single-basin tidal range power plants have the advantage of predictable energy outputs, but feature non-generation periods in every tidal cycle to facilitate the essential turbine driving head difference. Linked-basin tidal power systems can reduce this variability and consistently generate power. However, as a concept the latter are under-studied with research and information on their potential performance relative to single-basin designs being limited. In an effort to address this, we outline the basic principles of linked-basin power plant operation and report results from their numerical simulation. Lagoon operational models are applied to gauge their capabilities relative to conventional, single-basin tidal power systems. A coastal ocean model (*Thetis*) has in turn been equipped with linked-basin modelling capabilities in addition to single-basin tidal power plant operation strategies. Simulations demonstrate that deployment of linked-basin systems can lead to non-generation times being substantially reduced at the expense of the overall energy output relative to conventional tidal lagoons and barrages. As an example, a hypothetical case is considered for a site in the Severn Estuary, UK. A linked-basin system is shown to be able to generate energy 80–100% of the time over a spring-neap cycle, but harnesses $\approx 30\%$ of the energy of an equivalent-area single-basin design.

Keywords: Linked-basin lagoon, Tidal range energy, Resource assessment, Numerical model

1. Introduction

Tidal energy is a renewable energy source that comes with near complete predictability as a result of the tide generating forces attributed primarily to the coupled Earth-Moon-Sun system. In coastal sites offering amplifying geographical features in the form of pronounced tidal stream currents and a high

*Corresponding author
Email address: a.angeloudis@ed.ac.uk (Athanasios Angeloudis)

tidal range it is becoming economically feasible to tap into substantial marine energy resources [1, 2]. As an example, a first array of tidal stream turbines has been installed in the Pentland Firth, Scotland, UK [3]). Interest in tidal range structures has also resurfaced following the construction of the Lake Sihwa tidal power station in South Korea [4], while tidal range energy sites in the Bristol Channel and the Severn Estuary [5, 6] have been identified for their potential [7].

Tidal range power plants regulate their constituent hydraulic structures (e.g. turbines and sluices) to facilitate head differences that when released drive flows through turbines, generating power. Theoretically, the maximum potential energy available from a tidal head difference H (m) is given in J by the classical study of Prandle [8] as:

$$E_{\max} = \frac{1}{2}\rho g A H^2, \tag{1}$$

where ρ is the fluid density (kg/m^3), g is the gravitational acceleration (m/s^2) and A is the impounded plan surface area (m^2). The strategy for harnessing this energy will depend upon site-specific constraints that will dictate the project design. As such, assessment of tidal range energy options prior to their development relies on numerical tools that simulate, predict and potentially optimise their operation. This has been demonstrated in preceding studies, such as by Bae et al. [4] for the Lake Sihwa tidal power station in South Korea, Zhou et al. [9] for the proposed Severn Barrage, UK, and Burrows et al. [10] for schemes in the Irish Sea. In particular, as demonstrated by the majority of tidal power plant studies [11], while facilitating the driving head differences ($H = \eta_{\mathrm{i}} - \eta_{\mathrm{o}}$) between opposite sides of an impoundment there are periods in any conventional (i.e. single-basin) tidal power plant when generation will not be permissible.

We thus provide extensions to a methodology on the assessment of single-basin tidal range structures to examine a simple type of a linked-basin system. Linked-basin systems form a subset of tidal energy technologies that are fundamentally designed to deliver more consistent or controlled power contributions to the electricity grid in comparison with single-basin designs.

2. Linked-basin tidal power plant background

The use of connected basins to control the energy captured from the tides is not a new concept. Preliminary schematics date back at least to the 18^{th} century when Bernard Forest de Belidor described several tidal lagoon designs to grind flour over a longer period of time than traditional tidal mills by using multiple bodies of water [12, 13]. The descriptions of thirteen multi-basin concepts have been summarised by Bernshtein [14], drawing information from earlier ideas since the 19^{th} century that exploit the predictability of the tide in an attempt to provide baseline power. However, only a single actual small-scale scheme of this type has been reported: the Haishan tidal power plant in China featuring a capacity of 0.25MW since 1975. Following the Haishan plant's construction, linked-basin tidal power systems have been considered for other locations such as

the Bay of Fundy [15] and even as part of Severn Estuary tidal power feasibility studies in the UK.

Van Walsum [16, 15] reported that linked-basin proposals were typically dismissed in favour of single-basin or paired/associated-basin configurations. This has been attributed to the lack of competitiveness of linked-basin schemes in terms of extracting the maximum amount of energy at the lowest unit cost. Linked-basin schemes instead generally aim to provide energy on-demand, supply base load power and/or serve as fuel-displacement energy mechanisms. Nonetheless, in a site-specific study of the Bay of Fundy [16] it was documented that linked-basin systems could be designed and operated at a unit-price competitive with conventional single-basin designs, assuming that the geographic setting is favourable. Specifically, if the localised coastline does not require a cost-prohibitive construction of extensive seawalls/dykes or excessive environmental mitigation/compensation measures.

Linked-basin systems have previously been studied at a conceptual level, e.g. in the absence of hydrodynamic modelling. Assessments therefore relied on analytical approaches or at best reduced-order operation modelling (i.e. 0-D modelling) [14, 15]. 0-D models are appropriate for preliminary assessments and optimisation analyses [17] but must be treated with caution as nonlinear hydrodynamic processes can be affected both in the far-field and in the immediate near-field [18]. These limitations together with advances in computational resources has driven the development of multi-dimensional (1-D, 2-D, 3-D) hydro-environmental models [19, 20] coupled with operation algorithms of single-basin power plants [21, 22, 23, 24]. Regionally-focused coastal model applications have demonstrated how 0-D models can overestimate the energy output by as much as 50% [25, 26, 10] depending on how prospective designs interfere with localised tidal dynamics. This represents an uncertainty over previous findings regarding linked-basin systems that did not acknowledge these effects or any recent improvements on turbine capabilities.

In light of current efforts towards a low-carbon economy and infrastructure, renewable energy sources such as solar, wind and wave have received much attention [27]. The majority of these are characterised by high levels of intermittency, thus presenting a formidable reliability challenge that often requires on-demand use of traditional carbon-intensive energy to fill in gaps during periods when renewable sources become unavailable. Linked-basin tidal energy concepts can in theory deliver reliable and near continuous energy from a low-carbon energy source. It thus becomes a timely exercise to revisit and evaluate their potential through contemporary operational and coastal modelling techniques.

3. Methodology

3.1. Operation simulations of tidal power plants

For tidal power plant operation simulations we employ: (a) a finite difference operational model based on the principles of mass-balance, and (b) the finite element-based coastal ocean model *Thetis* that solves the depth-averaged shallow water equations. Details of these tools in the context of single-basin tidal

power plant assessment and optimisation are described in Angeloudis et al. [23]. We summarise the most salient details of the formulations applied here for linked-basin systems.

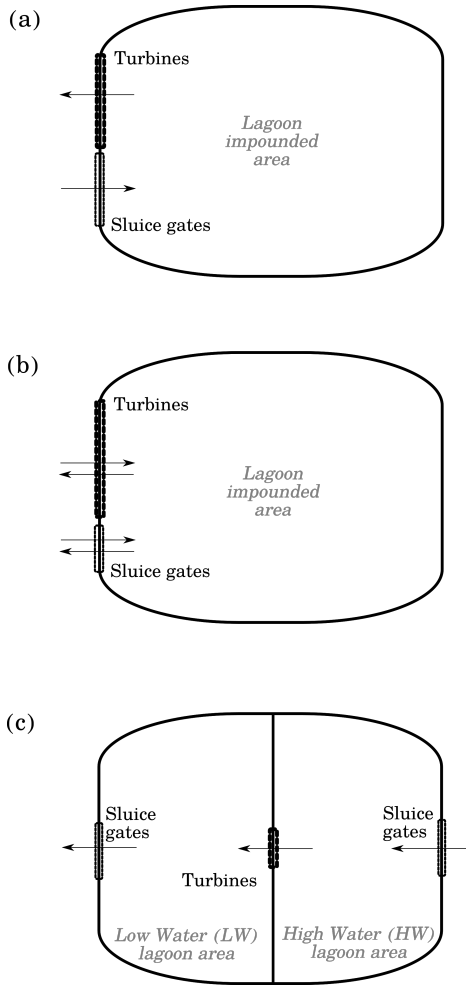

Figure 1: Tidal range power plant concepts: (a) single-basin ebb-only, (b) single-basin two-way and (c) linked-basin operation designs

3.1.1. Conventional tidal range plant operation

There is a wealth of information on the operation of conventional, single-basin power plants [11]. Their design entails the distribution of turbines and sluice gates along an impoundment that encloses an area where water volumes will be used for power generation (Fig. 1a,b). The plant operation can be either one-way (ebb-generation-only/flood-generation-only, Fig. 2a), two-way (bidirectional generation, Fig. 2b) and even include pumping intervals that can be used

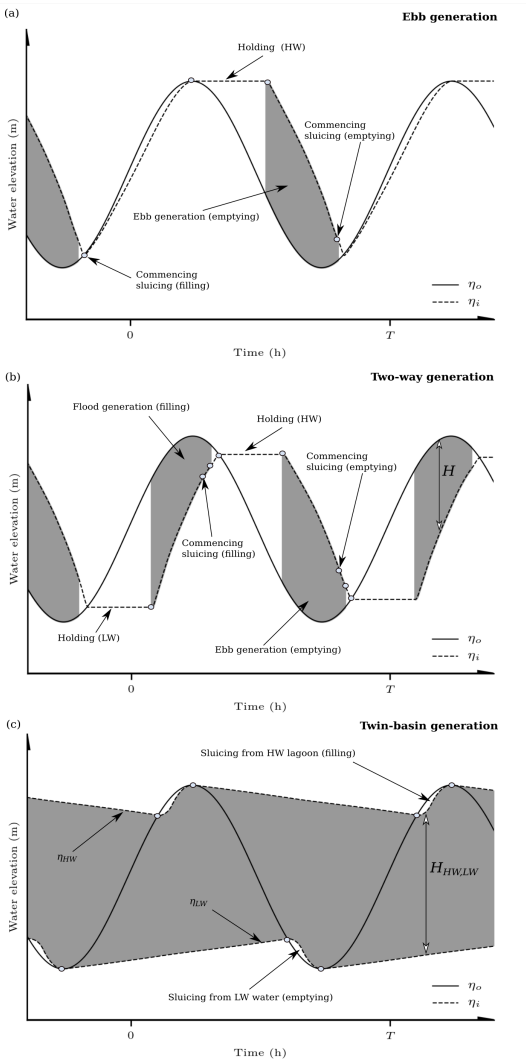

Figure 2: Operation of a tidal power plant over an M_2 tidal period, illustrating typical modes of operation. (a) Conventional one-way ebb generation, (b) two-way generation and (c) twin-basin generation. The dark grey sections indicate the periods when H drives power generation from the turbines.

to provide partial flexibility over generation times and/or an overall increase in energy yield. Irrespective of the above and as introduced previously, the duration of no-generation periods will depend on the tidal conditions (e.g. resulting from the significant variability over spring-neap cycles) as well as turbine constraints and capabilities [22]. Fig. 2a,b illustrates the general sequence for ebb and two-way operation, highlighting the periods when there is a sufficient head difference to drive the turbines (*in grey*). Additional details on the formulations

and sequences that dictate the operation have been reported in earlier work [23] and are omitted here for brevity. Effectively, the control of single-basin tidal power plants depends solely on the difference between the inner (η_i) and outer water levels (η_o) in close proximity to the hydraulic structures.

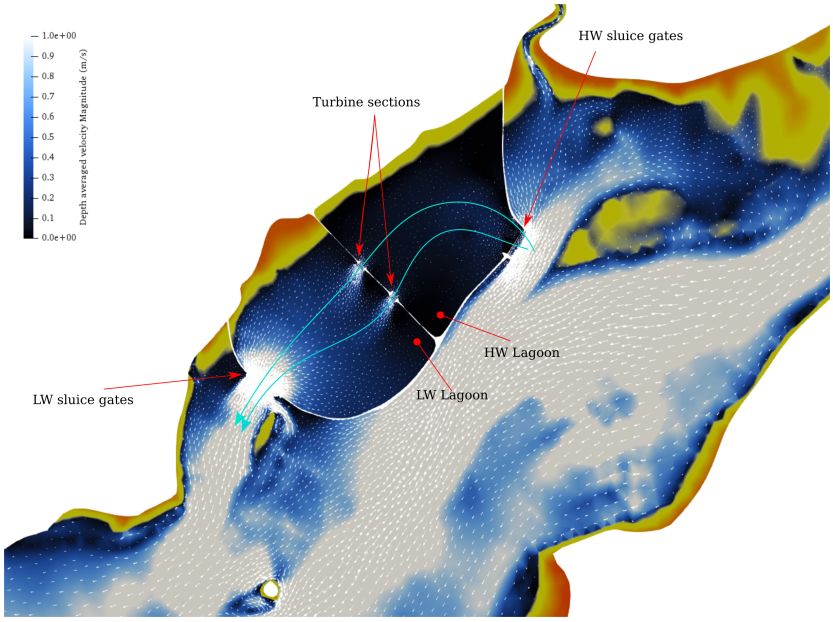

Figure 3: A practical example of a hypothetical twin-basin system that is discussed in detail later in this study. Shades of blue colour and vectors demonstrate instantaneous velocities from the operation of a hypothetical twin-basin system. The teal coloured trajectories illustrate indicative flow paths through the twin-basin system, passing first through the high and then the low water lagoons. Yellow/red regions indicate the dry areas within intertidal zones at the particular point in time.

3.1.2. Linked-basin lagoon operation

In their simplest form, linked-basin systems feature two lagoons that are internally connected, as in Fig. 1c. The operation in time is illustrated in Fig. 2c demonstrating how a sufficient head difference H can be theoretically maintained to generate continuously. All turbines are distributed at an internal barrier splitting the impounded area into two lagoons. The two lagoons are separately connected to the sea through independent sluice gate sections. Contrary to single-basin plants, three head differences must be considered: (a) one between the lagoons' two inner water levels at the turbine sections where H will dictate the flow and power generated and (b) the two values between each individual lagoon's inner and seaward (outer) elevations at the sluice gate sections. A practical example of a twin-basin system that is later discussed in the results section of this paper is depicted in Fig. 3. Initially, seawater enters a *High Water (HW)* lagoon where sluice gates are regulated to maintain as high a

water level as possible. In the example of Fig. 3 this corresponds to the northern impounded area. The increased water elevation in the HW lagoon can be observed by the shoreline location which is positioned further inland relative to the other, *Low Water (LW)* lagoon. The sluice gate discharge for the incoming flow in the HW lagoon ($Q_{s,HW}$) is calculated using the orifice equation as:

$$Q_{s,HW}(H_{HW,o}) = \begin{cases} r(t) \cdot C_d \cdot A_{s,HW} \cdot \sqrt{2g|H_{HW,o}|} & \text{for } H_{HW,o} > 0.0 \\ 0 & \text{for } H_{HW,o} \leq 0.0 \end{cases} \quad (2)$$

where $A_{s,HW}$ is the aggregate cross-sectional flow area (in m^2) of the gates installed, C_d is the sluice gate discharge coefficient [28], and $H_{HW,o}$ is the head difference of the HW lagoon inner water level and the outer water level at the sluice gate location. $r(t)$ is a ramp function that is introduced for numerical stability and a practical representation of the opening and closing of the hydraulic structures [9]. Additionally, there is a *Low Water (LW)* lagoon where water is maintained at as low a value as possible (in Fig. 3 the LW lagoon is the southern impounded area). The LW lagoon sluice gate discharge to release water back into the sea ($Q_{s,LW}$) is described by

$$Q_{s,LW}(H_{LW,i}) = \begin{cases} -r(t) \cdot C_d \cdot A_{s,LW} \cdot \sqrt{2g|H_{LW,o}|} & \text{for } H_{LW,o} < 0.0 \\ 0 & \text{for } H_{LW,o} \geq 0.0 \end{cases} \quad (3)$$

with $A_{s,LW}$ is the aggregate cross-sectional flow area (in m^2) of the LW lagoon sluice gates and $H_{LW,o}$ is the head difference between the LW lagoon inner water level and the outer water level at the sluice gate location. The primary objective of the sluice gates is to maintain a head difference ($H_{HW,LW}$) across the turbine sections of the internal lagoon barrier. The turbine flowrate Q_t and power output P can be sequentially calculated as:

$$Q_t(H_{HW,LW}) = \begin{cases} r(t) \cdot N_t \cdot Q_h(H_{HW,LW}) & \text{for } H_{HW,LW} \geq h_{\min} \\ 0 & \text{for } H_{HW,LW} < h_{\min} \end{cases} \quad (4)$$

$$P(H_{HW,LW}) = \begin{cases} r(t) \cdot N_t \cdot P_h(H_{HW,LW}) & \text{for } H_{HW,LW} \geq h_{\min} \\ 0 & \text{for } H_{HW,LW} < h_{\min} \end{cases} \quad (5)$$

where N_t is the number of turbines. Q_h and P_h correspond to the turbine flow and power of individual turbines determined according to the parametrisation of Table 1. As such, taking Fig. 3 as an example, the sea water flows through the twin basin system follows a consistent trajectory whereby it (a) enters through the HW sluice gates, (b) flows through the turbines between the HW and LW lagoons, generating energy, and (c) returns to the sea as the tide ebbs through the LW lagoon sluice gates.

Table 1: Parametrisation of a double-regulated bulb turbine applied in the tidal range energy resource assessments to calculate Power P_h and Discharge Q_h. Adapted from [23].

#	Formulations	Description
1	$S_p = \frac{2 \cdot 60 \cdot f_g}{G_p}$	Turbine speed S_p (rpm), where f_g is the grid frequency (Hz) and G_p the generator pole number.
2	$n_{11} = \frac{S_p \cdot D}{\sqrt{\lvert H \rvert}}$	Unit speed n_{11} (rpm) where D is the diameter (m).
3	$Q_{11} = \begin{cases} 0.017 n_{11} + 0.49, & n_{11} \leq 255 \\ 4.75, & n_{11} > 255 \end{cases}$	Unit discharge Q_{11} from empirical equations of [17].
4	$Q^* = Q_{11} D^2 \sqrt{\lvert H \rvert}$	Discharge estimate Q^* (m^3/s) through turbine for H (m).
5	$P^* = \mathbf{min}(\rho g Q^* \lvert H \rvert, C_p)$	Power for Q^* subject to the turbine capacity C_p (MW).
6	$Q_h = \frac{P^*}{\rho g \lvert H \rvert}$	Correction of $Q*$ to determine Q_h in case of maximum capacity C_p.
7	$\eta_h = -0.0019 n_{11} + 1.2461$	Empirical expression for hydraulic efficiency η_h[22].
8	$\eta_o = \eta_1 \cdot \eta_2 \cdot \ldots \cdot \eta_{n-1} \cdot \eta_n$	Consideration of other efficiency factors, e.g. turbine orientation, friction.
9	$P_h = \rho g Q_h \lvert H \rvert \eta_o$	Power P_h (MW) calculated subject to efficiency losses.

3.2. Tidal power plant design & operation optimisation

In the operation of tidal power plants one must consider differences among alternative design objectives. Single-basin power plants acknowledge the variability of the generation periods and the primary objective has typically been to maximise the energy output rather than opting for a continuous generation profile. In the case of twin-basin systems, consistent power contributions become a priority. The differences between design objectives are highlighted by the functionals used for the respective optimisation of the configurations below. The optimisation problems presented were solved either by using brute force for certain idealised cases or through the SciPy implementation of the L-BFGS-B algorithm building on earlier studies of the operational optimisation of tidal power plants [23].

3.2.1. Single-basin power plant energy maximisation

The operation of hydraulic structures and the duration of the individual modes (Fig. 2) in single-basin power plants can be varied, and thus optimised, subject to operational objectives and the current state of the transient tides. In order to pose a mathematical optimisation problem, we can encode the duration of the individual operation modes (e.g. the holding and sluicing duration on ebb/flood tides) in a vector, $\boldsymbol{\tau} = \{t_i,\, i = 1, \ldots, N\}$, where N is the number of control variables over the simulation period spanning t_s. As such, the following functional can be formed with the objective of finding an optimal $\boldsymbol{\tau}$ as well as

the turbine number N_t:

$$\begin{aligned} &\max && f(\boldsymbol{\tau}, N_t) = I_o(\boldsymbol{\tau}, N_t) - C_o(N_t) \\ &\text{subject to :} && \\ & && \boldsymbol{\tau}_l \leq \boldsymbol{\tau} \leq \boldsymbol{\tau}_u \\ & && 0.0 \leq N_t \times l_t \leq L \end{aligned} \tag{6}$$

where L is the available impoundment length for the placement of hydraulic structures (m), l_t is the length occupied by individual turbines (m). The vectors $\boldsymbol{\tau}_l$ and $\boldsymbol{\tau}_u$ refers to the lower and upper bounds expected for the different modes of operation. For simplicity, we relate the sluice gate number with N_t through the expression $N_s = (L - N_t \times l_t) \times h_s/A_s$. h_s is the cross-sectional height of the sluice gates installed and the ratio of h_s/A_s represents the sluice gate area per unit length in the assumption that the available hydraulic structure length not utilised by turbines is occupied by sluice gates. The optimisation functional defined above is formulated as the difference between operation revenue I_o (e.g. in £) and maintenance cost C_o (£) over a simulation period t_s. These can be calculated as

$$I_o(\boldsymbol{\tau}, N_t) = \int_{t_0}^{t_s} V_e P(\boldsymbol{\tau}, N_t)\, dt, \tag{7}$$

$$C_o(N_t) = \int_{t_0}^{t_s} V_o N_t C_p\, dt, \tag{8}$$

where V_e and V_o correspond to indicative values for the energy (e.g. in £/MWh) and an associated operational and maintenance cost per unit capacity installed (e.g. in £/MW). The C_o quantity defined by Eq.(8) is introduced to factor in the additional operation and maintenance costs associated with replacing sluice gates with a higher number and/or different types of turbine designs. C_p is the capacity of the installed turbines. For the 20 MW turbines considered in this work values of $V_o = 2.5$ and 3.125 £/MW/h are assumed for one-way or bidirectional configurations respectively, with the latter value being higher as this scenario is expected to require more maintenance. Note that these values are indicative and based on earlier technical reports [29, 30] that discuss the typical costs of tidal range energy.

3.2.2. Twin-basin power plant performance optimisation

In the case of twin-basin systems we expand the optimisation functional defined above such that it incorporates the standard deviation of the capacity factor ($CF = P/C_p$) over the simulation time. This is motivated by the desire to encourage a balance between energy maximisation and consistency. The standard deviation is denoted here as σ_P and the functional is expressed as

follows:

$$\begin{aligned} &\max && f(N_t) = \frac{1}{1+\beta\sigma_P} I_o(N_t) - C_o(N_t) \\ &\text{subject to :} && \\ & && 0.0 \leq N_t \times l_t \leq L \end{aligned} \tag{9}$$

where β is a weighting factor applied to amplify the significance of continuous power output at the expense of the overall energy produced. An additional difference in comparison with the functional defined in Eq. (6) is that the vector $\boldsymbol{\tau}$ is no longer applicable, with the only control parameter in this case being N_t. In achieving a consistent power output, the algorithm here, rather than controlling the flow through turbines to deliver a uniform amount of energy, aims to maintain a head difference H that is greater than the turbine rated head difference [22]. This in turn enables the installed turbines to generate power at their maximum generation capacity. The hill chart parametrisations (see Table 1) assume that turbines always operate at their peak possible efficiency and do not account for potential tuning capabilities in the absence of commercially sensitive details from turbine manufacturers.

3.3. Hydrodynamic Modelling

Thetis (`http://thetisproject.org/`) is a 2-D/3-D flow solver for simulating coastal and estuarine flows implemented using the *Firedrake* finite element Partial Differential Equation (PDE) solver framework [31, 32]. For this work we consider the non-conservative form of the nonlinear shallow water equations:

$$\frac{\partial \eta}{\partial t} + \nabla \cdot (H_d \mathbf{u}) = 0, \tag{10}$$

$$\frac{\partial \mathbf{u}}{\partial t} + \mathbf{u} \cdot \nabla \mathbf{u} - \nu \nabla^2 \mathbf{u} + f\mathbf{u}^{\perp} + g\nabla\eta = -\frac{\tau_b}{\rho H_d}, \tag{11}$$

where η is the water elevation, H_d is the total water depth and $\mathbf{u}$ is the depth-averaged velocity vector, and ν is the kinematic viscosity of the fluid. The term $f\mathbf{u}^{\perp}$ represents the Coriolis "force", where $\mathbf{u}^{\perp}$ is the velocity vector rotated counter-clockwise over 90^o and $f = 2\Omega\sin(\zeta)$ with Ω the angular frequency of the Earth's rotation and ζ the latitude. Bed shear stress (τ_b) effects are represented in the current applications through Manning's n formulation as:

$$\frac{\tau_b}{\rho} = g n^2 \frac{|\mathbf{u}|\mathbf{u}}{H_d^{\frac{1}{3}}}. \tag{12}$$

Intertidal processes are treated using the wetting and drying formulation detailed in Karna et al. [33]. The model itself is configured to use a discontinuous Galerkin finite element spatial discretisation (DG-FEM) and a semi-implicit Crank-Nicolson timestepping approach for the temporal discretisation. The

representation of turbines and sluice gates is implemented through the domain decomposition approach outlined in Angeloudis et al. [21]. Essentially, hydraulic structure fluxes linking subdomains are determined by sampling water elevations to calculate H values that feed into the hydraulic structure parametrisations (i.e. Eq. 2–5 and Table 1). The nonlinear discretised shallow water equations are iteratively solved with Newton's algorithm using the PETSc library [34].

4. Comparison between single-basin and linked-basin systems

The assessment of the linked-basin power plant concept is conducted in two stages through comparisons with results from conventional single-basin power plants. Firstly, idealised 0-D scenarios are considered to gauge the sensitivity of the plant performance to the tidal range and the hydraulic structure configuration. Subsequently we detail results from operational (0-D) and hydrodynamic (2-D) models that compare a proposed single-basin tidal lagoon design against a hypothetical linked-basin system in the Severn Estuary, UK.

4.1. Idealised tidal range structures

We consider an idealised setup for a tidal range structure that, for simplicity, is assumed to have a fixed surface area A and is not susceptible to intertidal effects. We assume that seaward (outer) elevations can be represented through a sinusoidal signal with a period of T= 12.42 h (i.e. an M_2 tidal period) and an amplitude defined by the parameter α. Four configurations are tested: (a) ebb-only generation, (b) two-way generation from a single-basin system and (c) linked-basin power plants with $\beta = 0$ and (d) $\beta = 25.0$. Sensitivity to the following is examined:

- The effect of the tidal amplitude (α) on the energy that can be extracted over an annual period. In principle, the potential energy available is determined from Eq. (1), with empirical estimates of 27% and 37% for ebb and two-way respectively, as per Burrows et al. [10]. However, more recent optimisation studies suggest that these fractions can vary [23].

- The significance of the impoundment length L that is available to position hydraulic structures. The sensitivity is based on a relationship $L = \lambda \times A$ where the value of λ is iteratively altered for a given impounded area A. While the resource for A can be quantified, the actual energy harnessed will invariably be constrained by site-specific characteristics on the placement of turbines and sluice gates (i.e. bathymetry, geomorphology and construction logistics) [35].

- The influence of the β factor in the linked-basin optimisation functional defined by Eq. (9). This is meant to assess for linked-basin systems the compromise on the overall energy that can be extracted if a more continuous generation profile is sought.

For simplicity, the operational control parameters for single-basin systems was explicitly specified. In ebb generation, the holding time was set to $t_{h,e} = 4.0$h; for two-way generation, $t_{h,e} = t_{h,f} = 3.0$h which are typical of the particular generation scheduling strategies though they can vary on a site specific basis [23]. The only variable remaining is the turbine number N_t and was determined through brute force optimisation.

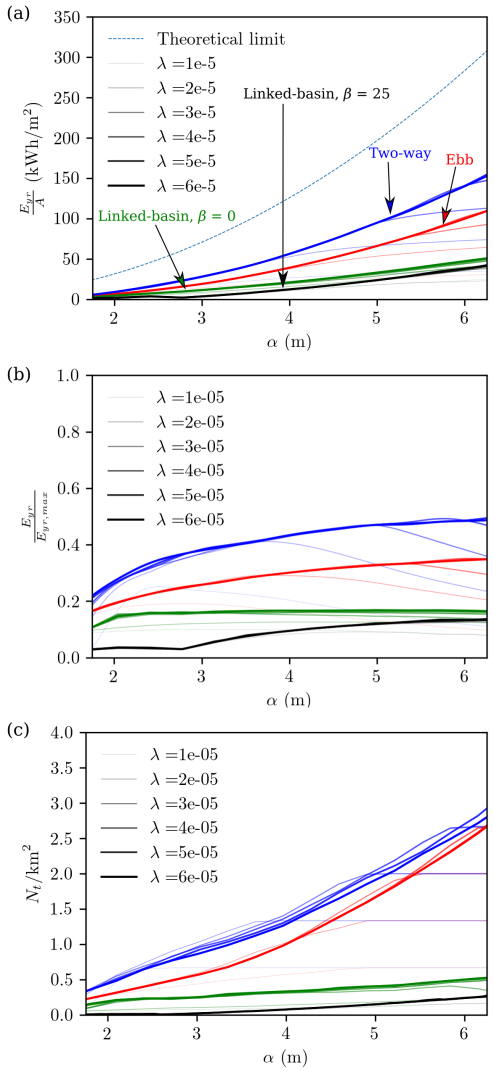

Figure 4: Sensitivity of idealised single-basin (*red* and *blue*) and linked-basin (*green* and **black**) configurations to amplitude. (a) Spatially normalised annual energy, (b) generation efficiency relative to maximum potential energy $\frac{E_{yr}}{E_{yr,max}}$, (c) normalised turbine number per area.

Results demonstrated that linked-basin systems produce substantially less energy than single-basin designs given the same area A (Fig. 4). As long as there is sufficient space allocated for turbines (λ), the plant efficiency for single-basin systems improves with an increasing tidal amplitude α. This is expected given the superior generation efficiency of bulb turbines for a greater head difference H [22]. Single-basin designs consistently require more turbines with the functional eventually opting to fully replace sluice gates with turbines as α increases. Specifically, in Fig. 4c only turbines, with zero sluice gates, are installed once N_t/km^2 transitions to a flat line. In contrast, linked-basin systems always require a significant distribution of sluice gates at the seaward sides since these are crucial to the power generated from the internal barrier (see Fig 4c).

For values of $\lambda = 6 \times 10^{-5}$ and $\alpha > 2$m, an idealised two-way configuration generates $\approx$ 30–50% of the theoretically available potential energy of Eq. 1. The ebb-only design follows with an equivalent $\approx$ 20–37% . A twin-basin scenario that is not constrained to generate continuously ($\beta = 0.0$) only captures $\approx 15\%$ of the resource. For a more consistent power output (i.e. $\beta = 25.0$) the efficiency reduces to $\approx$ 3–14% (Fig. 4b). As the parametrisation of Table 1 determines for a given H the maximum energy and flow through the turbines, a consistent power output is only facilitated once the head difference can be sustained to values greater than the turbine's rated head (in this case $H_r = 5.0$). As such, N_t for the linked-basin configuration with $\beta = 25.0$ is increased once $\alpha > 3$ m (see Fig. 4c) as it leads to a sustained head difference $H \geq 5$m.

Fig. 4c also demonstrates that even though twin-basin systems extract a lower fraction of the available energy, they require far less turbines to be installed which can correspond to a lower installation and maintenance cost, even though more sluice gates will be required. This sensitivity assessment sheds light on some generic characteristics of the performance of the configurations described in Fig. 1, excluding many of the factors that will additionally influence the operation performance in practice.

4.2. A practical application within the Severn Estuary, UK

The water elevations η at any site of practical relevance will be characterised by a variability resulting from multiple local tidal constituents. These constituents dictate the longer spring-neap (and other) cycles that lead to a gradually varying tidal range over time. In addition to these, hydrodynamics, wind, waves and even storm surge events [20] will also play a role on the tidal elevations experienced by a power plant.

As an example, we start from a proposal by Tidal Lagoon Power Ltd (TLP) for a Cardiff Lagoon; this would be a tidal range structure occupying an area of $\approx$ 66 km^2 within the Severn Estuary, UK. Preceding modelling studies associated with this particular site have focused on assessing and optimising the operation of what is a single-basin design [25] using a general arrangement stemming from publicly available data [36] as indicated in Fig. 5(c). Additionally here we assume a hypothetical linked-basin system in the same location as a

modification of the original single-basin outline and configuration to ensure hydraulic structures are positioned in areas of sufficient depth (see Fig. 5d) [35]. The two lagoons making up the linked-basin system split the site into two approximately equal surface area basins of 33 km^2 each.

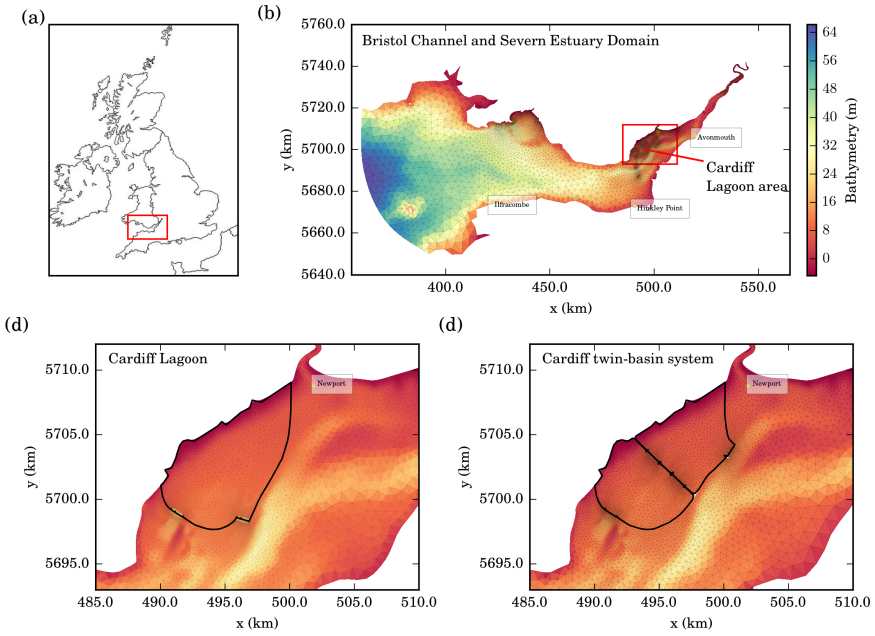

Figure 5: (a) Study area relative to UK map, (b) computational domain considered for the simulations in the Bristol Channel and the Severn Estuary, (c) Cardiff Lagoon and (d) Cardiff twin-basin system and unstructured mesh refinement.

The unstructured meshes generated using *qmesh* [37] and employed for the hydrodynamics simulations of the single- and linked-basin systems in the Severn Estuary are overlayed in Fig. 5. The baseline simulation's unstructured mesh comprised 20,666 nodes and 41,342 elements and was setup to simulate the tidal hydrodynamics over the period of a month beginning on the 6^{th} of May 2003. This was preceded by a 5-day simulation period that allowed the model to spin-up and become independent of the initial equilibrium conditions. Hydrodynamic models were forced at the seaward and inland boundaries using eight constituents from the TPXO database [38] and mean river flows from the UK's National River Flow Archive respectively. For the baseline scenario satisfactory agreement was demonstrated for the amplitudes and phases of the major constituents as summarised in Fig. 6; more details on the validation of *Thetis* models for the particular region can be found in Angeloudis et al. [23].

Water elevation time series predicted at the hydraulic structure locations

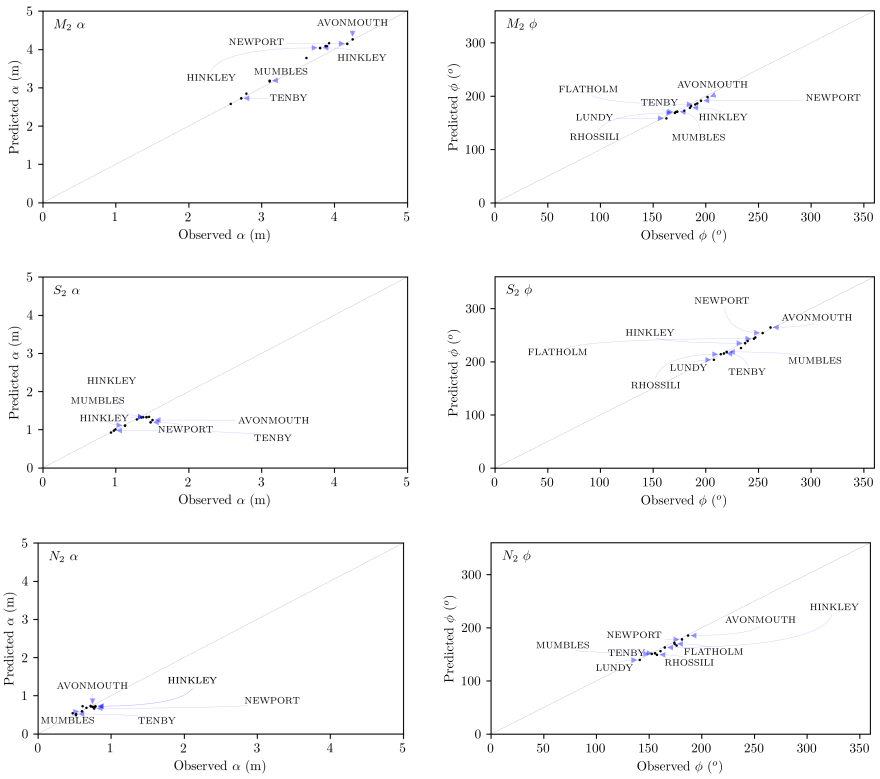

Figure 6: Comparison between predicted and observed tidal amplitude data for the three major tidal constituents in the region (M_2, S_2 and N_2) for the baseline Bristol Channel and Severn Estuary model.

for the simulated month were harmonically analysed in order to reconstruct extended time-elevation signals. These signals were used as inputs for the 0-D model as a representation of the seaward elevations at sluice gate and turbine sections. In addition, bathymetric data from the Edina Digimap Service [39] was employed to produce the plan surface area vs head difference relationships to parametrise the change in area due to intertidal effects in 0-D, assuming a constant elevation in the tidal power plant plan surface area [8].

Hydrodynamic modelling of the tidal range structure operation (Fig. 5c,d) entailed the refinement of the baseline setup in the proximity of hydraulic structures and the domain was split into subdomains that were configured to be connected through coupled open flux boundaries as per the domain decomposition method described previously [21].

4.2.1. Tidal power plant configurations

The turbine and sluice gate configuration for the single-basin design was initially determined by optimising the functional defined in Eq. 6 for both

the ebb-only and two-way generation cases. The optimisation was constrained by a hydraulic structure length of $L = 2200$m (corresponding to a value of $\lambda \approx 3 \times 10^{-5}$ in the idealised sensitivity study described in Section 4.1) chosen to be consistent with the outlines from TLP [36] and an annual simulation duration beginning from the 6^{th} of May 2003. Optimisation results converged to a capacity of 1960 MW which is within the range of 1800–2800 MW proposed. This corresponds to 98×20 MW turbines of diameter $D = 7.35$m and 48×150 m^2 sluice gates. For a scenario assuming control parameters remain fixed over the simulation period, ebb-generation converged to a holding time of $t_{h,e} = 4.10$ h, whereas for two-way generation there was an ebb-holding period of $t_{h,e} = 3.41$ h and a flood-holding period of $t_{h,f} = 2.30$ h respectively. An equivalent approach was applied for the hypothetical twin-basin system using the functional defined in Eq. 9 and a value of $\beta = 0.0$. The resultant configuration was 24×20 MW turbines i.e. a capacity C_p of 480 MW and 110 sluice gates over an accumulated hydraulic structure length of $L = 2200$m, consistent with the single-basin design. The turbine and sluice gate configurations were assumed fixed for all the operational cases summarised in Table 2. These practical setups were designed to demonstrate:

- differences in the generation profile resulting from the operation strategy selected in single-basin designs (Table 2, cases 1–2);
- benefits of adapting the operation control of single-basin designs over time subject to the transient tidal conditions (Table 2, cases 1–4);
- implications of aiming to generate continuously using a fixed number of turbines in linked-basin systems (Table 2, cases 5–7);
- impact of adjusting the number of turbines operating in order to sustain a continuous generation profile over certain periods (Table 2, cases 8–10);
- variations in electricity output based on the selected configurations.

Table 2: Single-basin and linked-basin cases considered for the assessment of twin-basin performance. $t_{h,e}$ = ebb holding period (h), $t_{h,f}$ = flood holding period, $N_{t,max}$ = maximum turbine number N_t that can be used.

#	ID	Type	Details	**Operation Description**
1	SB-EBB-C	Single-basin	$t_{h,e} = 4.10$h, $t_{h,f} = 0.00$h	Fixed control ebb-only
2	SB-TW-C	Single-basin	$t_{h,e} = 3.41$h, $t_{h,f} = 2.30$h	Fixed control two-way
3	SB-EBB-A	Single-basin	Variable $t_{h,e}$	Adaptive $\boldsymbol{\tau}$ for ebb-only
4	SB-TW-A	Single-basin	Variable $t_{h,e}, t_{h,f}$	Adaptive $\boldsymbol{\tau}$ for two-way
5	LB-$N_t = 4$	Linked-basin	$N_t = 4$	Fixed N_t throughout
6	LB-$N_t = 10$	Linked-basin	$N_t = 10$	Fixed N_t throughout
7	LB-$N_t = 24$	Linked-basin	$N_t = 24$	Fixed N_t throughout
8	LB-$\beta = 5.0$	Linked-basin	$N_{t,\max} = 25$, $\beta = 5.0$	Adaptive N_t based on β
9	LB-$\beta = 10.0$	Linked-basin	$N_{t,\max} = 25$, $\beta = 10.0$	Adaptive N_t based on β
10	LB-$\beta = 25.0$	Linked-basin	$N_{t,\max} = 25$, $\beta = 25.0$	Adaptive N_t based on β

The 'adaptive' operation strategies (summarised in Table 2) consider the temporal variability of the tides. This is achieved by initially solving the optimisation problems defined by the functionals given in Eqs. 6 and 9 for every individual tidal cycle to determine varying control parameters as the tide evolves. For single-basin scenarios, holding periods $(t_{h,e}, t_{h,f})$ are recursively updated in every tidal period. In linked-basin system scenarios, the number of operational turbines N_t is regulated in an attempt to maintain consistent power outputs for each tidal cycle dependent on the β factor.

4.2.2. Operational modelling results

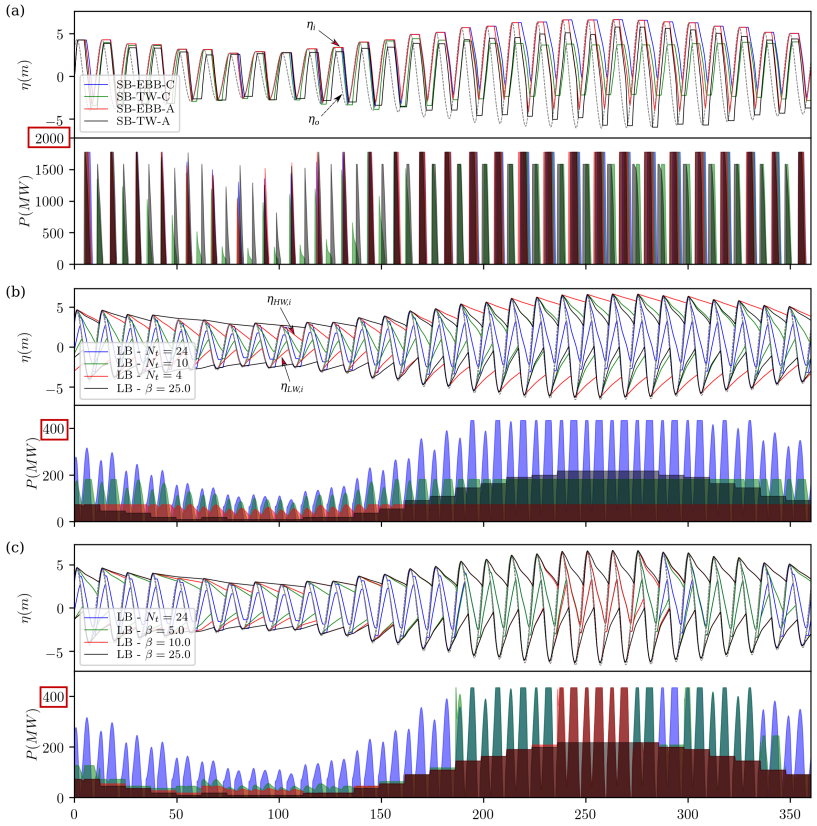

Figure 7: Elevations and power output through 0D operation simulations of single- and linked-basin cases over a spring-neap cycle. (a) Comparison of single-basin cases; (b) comparison of linked-basin cases using a fixed number of turbines (and including the adaptive operation linked-basin case with $\beta = 25.0$ (LB-$\beta = 25.0$); (c) comparison of linked-basin cases adapting the number of operational turbines temporally (including a case where the number of operational turbines remains fixed LB-$N_t = 24$).

An overview of the tidal power plant 0-D simulation results is summarised in Table 3. Firstly, single-basin plant normalised energy outputs for fixed control

configurations (SB-EBB-C, SB-TW-C) are consistent (29.8% and 36.9%) with practical estimates from other models [10] of 27% and 37% for ebb-only and two-way generation respectively. The operational optimisation in the adaptive setups delivers improved performance which is merely marginal and below 1% for ebb-only generation (SB-EBB-A) as only a single scheduling parameter is allowed to vary (ebb holding period) with no significant impact on the output. However, the performance improvement in the two-way generation (SB-TW-A) following optimisation is more substantial ($\approx 5\%$). Ebb-only configurations generate ≈26.5% of the time whereas two-way setups generate for ≈43.5% of the time. There are discernible patterns in the generation profile of configurations using adaptive controls, as the holding periods during neap tides tend to be prolonged in order to maximise H prior to turbining, leading to greater power peaks over shorter generation intervals. In contrast, over spring tides when greater H values can be sustained for longer, operation holding periods are shortened, leading to longer generation periods as observed in Fig. 7a.

Table 3: 0-D operational model power output predictions. $E_{yr,0D}$ = 0-D predicted annual energy output, $E_{\max}$ = maximum theoretical energy available (1), $|CF|$ = average capacity factor throughout the year. Availability is defined as the proportion of time with non-zero generation.

Configuration	$E_{yr,0D}$ (TWh)	$E_{yr,0D}/E_{\max}$ (%)	$\|CF\|$ (%)	Availability (%)
SB-EBB-C	3.131	29.8	18.2	26.4
SB-EBB-A	3.180	30.3	18.5	26.7
SB-TW-C	3.871	36.9	22.6	42.8
SB-TW-A	4.558	43.4	26.6	44.1
LB-$N_t = 4$	0.566	5.4	80.7	100.0
LB-$N_t = 10$	1.061	10.1	60.6	97.6
LB-$N_t = 24$	1.354	12.9	30.9	80.1
LB-$\beta = 5.0$	1.040	9.9	23.7	97.4
LB-$\beta = 10.0$	0.732	6.9	16.7	99.9
LB-$\beta = 25.0$	0.630	6.0	27.7	100.0

Practical linked-basin energy outputs are notably worse relative to single-basin cases. The best scenario in terms of energy performance (LB-$N_t = 24$) extracts 42.5% and 29.7% of the optimised ebb (SB-EBB-A) and two-way (SB-TW-A) configurations respectively. However, the particular linked-basin system has an availability of only 80% as the use of N_t =24 turbines leads to a rapid depletion of H between the two basins resulting in frequent no-generation periods (Fig. 7b, *blue* lines). Reducing the number of turbines (LB-N_t =10) allows a continuous generation during spring tides, but not over neap tides as the reduced tidal range does not yield the necessary water volume in the HW lagoon to sustain a value of H greater than the turbine rated head indefinitely (Fig. 7b, *green* lines).

The concept of regulating the number of operational turbines in the adaptive linked-basin configurations returns interesting results. The power generation profiles in Fig. 7c suggest that as β is increased, the number of operational

turbines at neap tides is reduced to limit the water volume exchange between HW and LW lagoons to preserve H and deliver a constant power output over every 12.42h period; this corresponds to a substantially reduced total power output during the period. As the tidal elevations transition to spring periods the number of operational turbines increases along with the power output. For low values of β (i.e in this case $\beta = 5$ and 10) even though the functional defined in Eq. 9 penalises the output based on its consistency, the algorithm converges to using all available turbines (i.e. $N_t = 24$). For $\beta = 25$, the power output remains constant for each tidal cycle period, with the number of turbines being successfully altered to follow the gradual changes in the tidal range. At no point does the number of turbines exceed N_t=14. The performance of these adaptive strategies in terms of energy output is below 10% of the potential energy, but they can provide continuous power and feature gradual transitions in the power produced between tidal cycles. The smoother transition in the power generation would potentially correspond to more manageable slew rates from an electronics point of view.

Insights into the generation profiles of single-basin and linked-basin options can be observed in Fig. 8 that illustrates the power generation averaged over the 705 tidal cycles comprising the simulated year. Ebb-only configurations feature on average the highest generation peak, followed by two-way configurations. There is a significant variance in the power generated by single-basin systems depending on the individual tidal cycle. In contrast, the variance is significantly lower for linked-basin systems (as illustrated for LB-$N_t = 4$, LB-$N_t = 10$ and LB-$\beta = 25$). Nevertheless, Fig. 8b clearly demonstrates that the power generated is substantially lower than for conventional tidal power plant designs.

Table 4: Comparison between 0-D and 2-D predictions for conventional and twin-basin systems considered. $E_{mth,0D}$ = Monthly 0-D simulation prediction, $E_{mth,2D}$ = Monthly 2-D simulation prediction

Configuration	$E_{mth,0D}$ (GWh)	$E_{mth,2D}$ (GWh)	$\frac{E_{mth,0D}-E_{mth,2D}}{E_{mth,0D}}$ (%)
SB-EBB-C	258.2	241.3	6.5
SB-EBB-A	260.2	233.3	10.3
SB-TW-C	319.4	308.2	3.5
SB-TW-A	367.8	349.4	5.0
LB-$N_t = 4$	46.6	48.3	-3.6
LB-$N_t = 10$	85.3	93.3	-9.4
LB-$N_t = 25$	108.9	97.3	10.6
LB-$\beta = 5.0$	76.9	75.6	1.6
LB-$\beta = 10.0$	58.6	58.9	-0.5
LB-$\beta = 25.0$	51.5	50.8	1.4

Thetis 2-D simulations were performed in order to establish whether the 0-D trends observed for the operation of alternative lagoon design options remain consistent once the effects of regional hydrodynamics are included (Table 4).

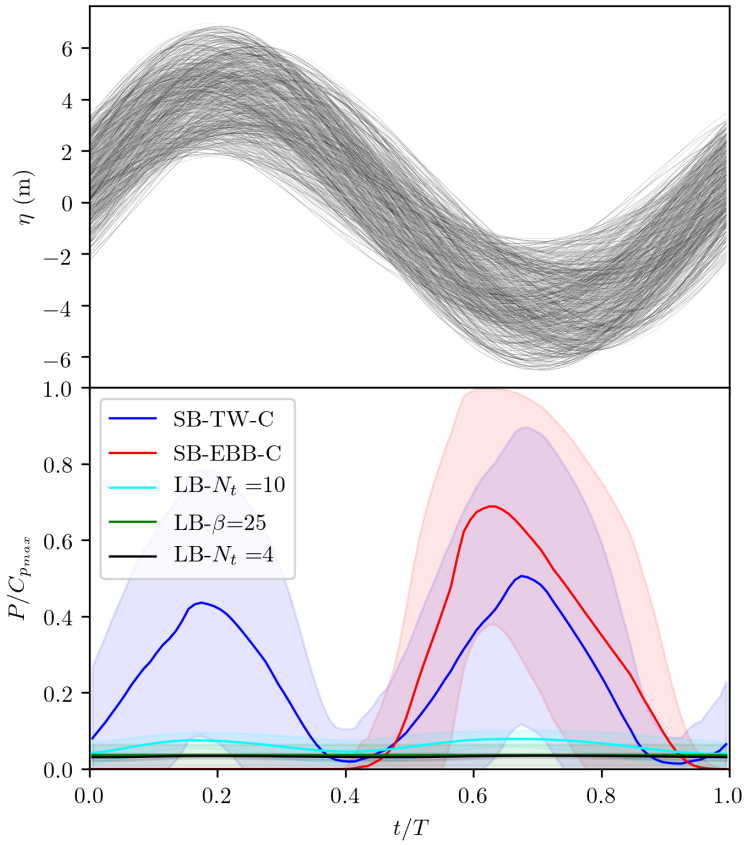

Figure 8: (a) Water elevations (η) for each of the 12.42h tidal cycles over a yearly period at the seaward side of the southern hydraulic structure section (top figure) and (b) average power-production over the tidal cycle period from annual 0-D simulations. Shaded areas illustrate the standard deviation of power produced at any point over the tidal cycle. $C_{p_{\max}}$ corresponds to the maximum capacity installed, i.e. 1960 MW for single-basin configurations.

This exercise aimed to ensure that the simplifications of the 0-D model are not compromising its predictive capabilities by ignoring hydrodynamic impacts that such infrastructure projects will incur [26, 10]. In all cases considered, energy output differences between 0-D and 2-D models are relatively small suggesting consistent conclusions can be drawn from both approaches. This reinforces the use of the 0-D model for the energy output assessment of both single-basin and linked-basin schemes, at least at the early design and assessment stages and for the conceptual development of similar tidal range energy designs. Hydro-

dynamic models are essential to address hydro-environmental implications and shed light into how tidal range power plants would function in practise. Fig. 3 illustrates an instantaneous velocity contour plot from *Thetis*, highlighting the general flow direction in the linked-basin system and also the general arrangement of the linked-basin system. In this case, as the shape and size of the linked-basin system closely follows the single-basin proposal of TLP's Cardiff Lagoon, a similar footprint is impacted on the seaward tidal constituents as with the previous modelling results of Angeloudis and Falconer [25]. The principal tidal constituents $M_2 \approx 4.17$ m and $S_2 \approx 1.47$ m would be reduced by 0.25 m and 0.12 m respectively, slightly affecting the pronounced tidal range in the Severn Estuary. Moreover, as the scheme acts as an obstruction to the otherwise unhindered basin, advective accelerations are noticeable as the flow is redirected to circumvent the impounded area. Inside the lagoons the average velocity magnitude reduces away from the hydraulic structures; however, since turbines are consistently operating and promoting mixing, water volumes within the linked-basin system would appear to be less prone to the effects of stagnation. These aspects should be more rigorously quantified by linking the hydrodynamic models with water quality and morphodynamics models, which are beyond the immediate scope of this study.

In terms of the energy outputs for both single-basin and linked-basin designs, further performance improvements could be realised if pumping periods are included. This entails the investment of energy to utilise turbines as pumping mechanisms at certain periods of the tidal cycle, leading to increases in the overall energy outputs of a scheme [40, 41]. However, as pumping is not featured in the particular linked-basin system configuration, it has been intentionally omitted from the analysis for simplicity. Nonetheless, a subset of linked-basin designs by Bernshtein [14] include the distribution of pumps across the impoundment to provide an additional, pumped storage function to the operation. For single-basin designs, operation featuring pumping intervals has already been applied in practice at the La Rance barrage in France. In addition, recent studies suggest that pumping could add substantial value to prospective tidal power plants, as it can offer additional flexibility opportunities for both maximising the energy outputs as well as the income from the plant operation [24].

5. Conclusions

This study is the first to present operational modelling results investigating the potential of linked-basin tidal range power systems relative to conventional, single-basin tidal range power plants. A particular incentive of linked-basin options is the potential to deliver continuous, low-carbon and renewable power to the electricity grid. However, we highlight that the varying tidal range can greatly influence the magnitude of the power that can be continually delivered.

To our knowledge the research presented is also the first study reporting on the performance of linked-basin systems using contemporary coastal modelling methods. Depth-averaged regional simulations demonstrate that a twin-basin

system could extract on average ≈ 30 % of the energy compared to a conventional tidal power plant occupying an equivalent plan surface area. Linked-basin designs could even feature hydro-environmental advantages that include the continuous exchange of water volumes between lagoons (avoiding stagnation) and deployment of a reduced number of turbines, which would also be positioned away from marine migratory routes. The latter is because only sluice gate hydraulic structures would be positioned on the seaward side of the impoundment.

Finally, the results suggest that linked-basin concepts are technically feasible according to the current turbine technologies available. However, the value of the consistent power that can be delivered, given the lower total energy output, remains questionable given recent advances and research on novel energy storage options.

Acknowledgements

A. Angeloudis acknowledges the support of the NERC Industrial Innovation fellowship grant NE/R013209/2. M. Piggott acknowledges the support of EPSRC under grants EP/M011054/1 and EP/R029423/1.

References

[1] A. G. Borthwick, Marine renewable energy seascape, Engineering 2 (2016) 69 – 78.

[2] M. Melikoglu, Current status and future of ocean energy sources: A global review, Ocean Engineering 148 (2018) 563 – 573.

[3] R. Martin-Short, J. Hill, S. Kramer, A. Avdis, P. Allison, M. Piggott, Tidal resource extraction in the pentland firth, uk: Potential impacts on flow regime and sediment transport in the inner sound of stroma, Renewable Energy 76 (2015) 596 – 607.

[4] Y. H. Bae, K. O. Kim, B. H. Choi, Lake Sihwa tidal power plant project, Ocean Engineering 37 (2010) 454–463.

[5] S. Waters, G. Aggidis, Tidal range technologies and state of the art in review, Renewable and Sustainable Energy Reviews 59 (2016) 514–529.

[6] M. Kadiri, R. Ahmadian, B. Bockelmann-Evans, W. Rauen, R. Falconer, A review of the potential water quality impacts of tidal renewable energy systems, Renewable and Sustainable Energy Reviews 16 (2012) 329–341.

[7] C. Hendry, The role of tidal lagoons, Technical Report, UK Government, 2017. URL: `https://hendryreview.com/`.

[8] D. Prandle, Simple theory for designing tidal power schemes, Advances in water resources 7 (1984) 21–27.

[9] J. Zhou, S. Pan, R. a. Falconer, Optimization modelling of the impacts of a Severn Barrage for a two-way generation scheme using a Continental Shelf model, Ren. Energy 72 (2014) 415–427.

[10] R. Burrows, I. Walkington, N. Yates, T. Hedges, J. Wolf, J. Holt, The tidal range energy potential of the West Coast of the United Kingdom, Applied Ocean Research 31 (2009) 229–238.

[11] S. P. Neill, A. Angeloudis, P. E. Robins, I. Walkington, S. L. Ward, I. Masters, M. J. Lewis, M. Piano, A. Avdis, M. D. Piggott, G. Aggidis, P. Evans, T. A. Adcock, A. Židonis, R. Ahmadian, R. Falconer, Tidal range energy resource and optimization – past perspectives and future challenges, Renewable Energy (2018) –.

[12] B. F. de Belidor, Architecture hydraulique ou l'art de conduire, d'élever et de ménager les eaux pour les différents besoins de la vie, volume 2, 1739.

[13] L. B. Bernshtein, Tidal power development-a realistic, justifiable and topical problem of today, IEEE Transactions on Energy Conversion 10 (1995) 591–599.

[14] L. B. Bernshtein, Tidal energy for electric power plants, Israel Program for Scientific Translations, Jerusalem, Israel, 1961.

[15] W. Van Walsum, Offshore Engineering For Tidal Power, in: The Ninth International Offshore and Polar Engineering Conference, International Society of Offshore and Polar Engineers, Brest, France, 1999, pp. 777–784.

[16] W. Van Walsum, Barriers to tidal power: multi basin plants, 2004. URL: http://www.waterpowermagazine.com/features/featurebarriers-to-tidal-power-multi-basin-plants/.

[17] G. Aggidis, D. Benzon, Operational optimisation of a tidal barrage across the Mersey estuary using 0-D modelling, Ocean Engineering 66 (2013) 69–81.

[18] R. A. Falconer, A. Angeloudis, R. Ahmadian, Modeling Hydro-environmental Impacts of Tidal Range Renewable Energy Projects in Coastal Waters, WORLD SCIENTIFIC, 2018, pp. 1553–1574. doi:10.1142/9789813204027_0055.

[19] J. Wolf, I. A. Walkington, J. Holt, R. Burrows, Environmental impacts of tidal power schemes, Proceedings of the ICE Maritime Engineering 162 (2009) 165–177.

[20] M. Lewis, A. Angeloudis, P. Robins, P. Evans, S. Neill, Influence of storm surge on tidal range energy, Energy 122 (2017) 25 – 36.

[21] A. Angeloudis, R. Falconer, S. Bray, R. Ahmadian, Representation and operation of tidal energy impoundments in a coastal hydrodynamic model, Renewable Energy 99 (2016) 1103–1115.

[22] G. Aggidis, O. Feather, Tidal range turbines and generation on the solway firth, Ren. Energy 43 (2012) 9 – 17.

[23] A. Angeloudis, S. C. Kramer, A. Avdis, M. D. Piggott, Optimising tidal range power plant operation, Applied Energy 212 (2018) 680 – 690.

[24] F. Harcourt, A. Angeloudis, M. D. Piggott, Utilising the flexible generation potential of tidal range power plants to optimise economic value, Applied Energy 237 (2019) 873 – 884.

[25] A. Angeloudis, R. A. Falconer, Sensitivity of tidal lagoon and barrage hydrodynamic impacts and energy outputs to operational characteristics, Ren. Energy 114(A) (2017) 337–351.

[26] N. Yates, I. Walkington, R. Burrows, J. Wolf, The energy gains realisable through pumping for tidal range energy schemes, Renewable Energy 58 (2013) 79–84.

[27] C. Pérez-Collazo, D. Greaves, G. Iglesias, A review of combined wave and offshore wind energy, Renewable and Sustainable Energy Reviews 42 (2015) 141 – 153.

[28] A. Baker, Tidal power, IEE Proceedings A Physical Science, Measurement and Instrumentation, Management and Education, Reviews 134 (1987) 392.

[29] Poyry, Levelised cost of power from tidal lagoons, A report to Tidal Lagoon Power Plc, 2014. Accessed: 15-10-2017.

[30] R. Burrows, I. Walkington, N. Yates, T. Hedges, J. Wolf, J. Holt, Tapping the Tidal Potential of the Eastern Irish Sea, Final Report, Joule Project JIRP106/03. University of Liverpool and Proudman Oceanographic Laboratory., 2009. URL: `http://www.liv.ac.uk/engineering/tidalpower`.

[31] F. Rathgeber, D. A. Ham, L. Mitchell, M. Lange, F. Luporini, A. T. T. Mcrae, G.-T. Bercea, G. R. Markall, P. H. J. Kelly, Firedrake: Automating the finite element method by composing abstractions, ACM Trans. Math. Softw. 43 (2016) 24:1–24:27.

[32] T. Kärnä, S. C. Kramer, L. Mitchell, D. A. Ham, M. D. Piggott, A. M. Baptista, Thetis coastal ocean model: discontinuous galerkin discretization for the three-dimensional hydrostatic equations, Geoscientific Model Development Discussions 2018 (2018) 1–36.

[33] T. Karna, B. de Brye, O. Gourgue, J. Lambrechts, R. Comblen, V. Legat, E. Deleersnijder, A fully implicit wetting–drying method for DG-FEM shallow water models, with an application to the Scheldt Estuary, Computer Methods in Applied Mechanics and Engineering 200 (2011) 509–524.

[34] S. Balay, S. Abhyankar, M. F. Adams, J. Brown, P. Brune, K. Buschelman, L. Dalcin, V. Eijkhout, W. D. Gropp, D. Kaushik, M. G. Knepley, L. C. McInnes, K. Rupp, B. F. Smith, S. Zampini, H. Zhang, H. Zhang, PETSc Users Manual, Technical Report ANL-95/11 - Revision 3.7, Argonne National Laboratory, 2016. URL: http://www.mcs.anl.gov/petsc.

[35] A. Angeloudis, R. Ahmadian, R. A. Falconer, B. Bockelmann-Evans, Numerical model simulations for optimisation of tidal lagoon schemes, Applied Energy 165 (2016) 522–536.

[36] TLP, Tidal Lagoon Power Cardiff Lagoon, http://www.tidallagoonpower.com/projects/cardiff/planning/, 2017. Accessed: 15-10-2017.

[37] A. Avdis, A. S. Candy, J. Hill, S. C. Kramer, M. D. Piggott, Efficient unstructured mesh generation for marine renewable energy applications, Renewable Energy 116 (2018) 842–856.

[38] G. D. Egbert, S. Y. Erofeeva, Efficient inverse modeling of barotropic ocean tides, Journal of Atmospheric and Oceanic Technology 19 (2002) 183–204.

[39] Edina Digimap Service, Hydrospatial one, gridded bathymetry, http://digimap.edina.ac.uk/marine/, 2014. , SeaZone Solutions Ltd, Online; accessed 2017.

[40] N. Yates, I. Walkington, R. Burrows, J. Wolf, Appraising the extractable tidal energy resource of the UK's western coastal waters, Phi. Trans. Royal Soc. A: Math. Phys. Eng. Sci. 371 (2013).

[41] A. Angeloudis, Tidal range structure operation assessment and optimisation, Dams and Reservoirs 0 (0) 1–10.